PHYSICAL REVIEW B **95**, 180104(R) (2017)

Broadband solid cloak for underwater acoustics

Yi Chen,[1] Mingye Zheng,[1] Xiaoning Liu,[1,*] Yafeng Bi,[2] Zhaoyong Sun,[2] Ping Xiang,[3] Jun Yang,[2] and Gengkai Hu[1,*]

[1]*Key Laboratory of Dynamics and Control of Flight Vehicle, Ministry of Education, School of Aerospace Engineering, Beijing Institute of Technology, Beijing 100081, China*

[2]*Key Laboratory of Noise and Vibration Research, Institute of Acoustics, Chinese Academy of Sciences, Beijing 100190, China*

[3]*System Engineering Research Institute, Beijing 100094, China*

(Received 8 December 2016; published 30 May 2017)

The application of transformation theory to underwater acoustics has been a challenging task because highly anisotropic density is unachievable in water. A possible strategy is to exploit the anisotropic modulus rather than density, although it has not been experimentally demonstrated. We present an annular underwater acoustic cloak designed from particular graded solid microstructures. The geometry tailored microstructures mimic metafluid with highly anisotropic modulus through substantially suppressed shear waves. Transient wave experiments are conducted with the cloak in a designed two-dimensional underwater waveguide system and proved excellent cloaking performance for an enclosed target over broadband frequencies 9–15 kHz. This finding paves the way for controlling underwater acoustics using the structured anisotropic modulus metafluid.

DOI: 10.1103/PhysRevB.95.180104

Inspired by the form invariance of Maxwell's equations under spatial mapping, a general transformation method [1,2] was proposed to control wave propagation accurately through material distribution. Invisible cloaks as ultimate applications have been realized for electromagnetic waves [3–9], flexural plate waves [10,11], thermal flux [12,13], and liquid surface waves [14] with contemporary metamaterials [15,16]. For the acoustic cloak, metafluid with anisotropic density [17,18], impossible in natural fluids, is required by the transformation approach. This has been realized with the perforated plate technique [19,20] for air sound. However, the cloak for underwater acoustics still faces significant challenges due to unavailable material design.

For air sound, the solid perforated plate can be treated as rigid and provides additional momentum along the orthogonal direction [19–22], which induces a density difference along two principal directions [19,20]. Unfortunately, no solid material [23] can be treated as rigid in water, and the stimulated shear waves in a solid will dramatically decrease the anisotropy [23,24]. Even for air sound, effective density in two principal directions with the technique can only differ by five times or less [22], which is not sufficiently large to build a cylindrical cloak. In addition, this metamaterial requires fluid as the working media [21–25] and is essentially fluidic with limited practical applications, such as mobility working conditions.

Since the anisotropic density metafluid is unworkable for an underwater acoustics cloak, a direct conjecture is to use a metafluid with anisotropic modulus instead of density. Although anisotropic density metafluid has been investigated extensively [19–25], few studies have been concerned with realizing anisotropic modulus metafluid. Indeed, anisotropic modulus is a rather common property in natural solids or artificial structures. Although solids differ from fluids essentially owing to coexisting longitudinal and shear waves, it is possible to decouple the two waves and obtain fluidlike materials with a single bulk wave through microstructure design [26,27], so as to separate the longitudinal and shear wave velocities stringently [28–30]. This concept coincides with long ago forwarded pentamode (PM) material [31], which was recognized recently [32] as one type of anisotropic modulus metafluid in regard to acoustics. Through the carefully tailored geometry of PM material, its effective shear to bulk modulus ratio (G/K) can be smaller than $1/1000$ in three dimensions (3D) [29] or $1/100$ in two dimensions (2D) [26], with the two principal moduli differing by 50 times [26], which mimics a strong anisotropic modulus metafluid. More importantly, the anisotropic modulus results from a quasistatic property without a resonance mechanism and works for an extreme broadband range [26] if the unit cell is sufficiently small. Since the modulus and density of common solids, such as aluminum, copper, or steel, is at the same order of magnitude as water, PM-type metafluid is especially suitable for controlling underwater acoustics [33–37]. Although PM material has numerically demonstrated its effectiveness as an anisotropic modulus fluid in underwater cloak [26], mirage [27], and metasurface applications [35], experiment validation has never been reported due to complicated microstructure design and difficulties in underwater acoustic measurements.

In this Rapid Communication, we present an underwater acoustic cloak with PM material and demonstrate experimentally its broadband cloaking performance. It should be noted that a cloak for underwater acoustics reported in Ref. [25] is designed from anisotropic density metamaterials and requires fluid as the necessary working media, while here only solid structures with a designed highly anisotropic modulus are needed. Due to the available strong anisotropy in the modulus through microstructure design, the material parameter for the cloak is not scaled as in previous examples [19,20] and is therefore impedance matched with background water. In addition, the fabricated cloak has a much smaller thickness relative to the inner radius [3,6,10,11], which is favorable for practical usage. Transient wave experiments were conducted in a specially designed two-dimensional (2D) underwater waveguide system and validated the superior wave shielding performance of the designed cloak, achieving an average 6.3 dB reduction of target strength over a broad frequency band range of 9–15 kHz.

*Corresponding authors: liuxn@bit.edu.cn and hugeng@bit.edu.cn

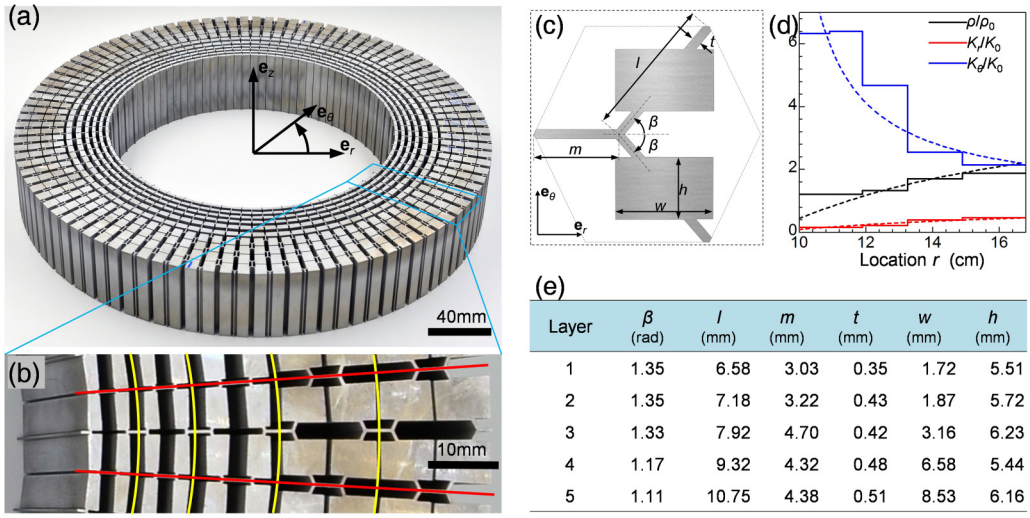

Layer	β (rad)	l (mm)	m (mm)	t (mm)	w (mm)	h (mm)
1	1.35	6.58	3.03	0.35	1.72	5.51
2	1.35	7.18	3.22	0.43	1.87	5.72
3	1.33	7.92	4.70	0.42	3.16	6.23
4	1.17	9.32	4.32	0.48	6.58	5.44
5	1.11	10.75	4.38	0.51	8.53	6.16

FIG. 1. Solid cloak designed from pentamode material. (a) Image of the cloak machined from an aluminum block with inner diameter 200 mm, outer diameter 334 mm, and height 50 mm, consisting of 500 hexagonal unit cells. (b) Enlarged view of one segment, highlighted in (a). Structure between red lines represents one sector in the θ direction and yellow lines separate the five graded unit cells. (c) Proposed pentamode unit cell with six geometric parameters, topology angle β, oblique and horizontal rib length l and m, rib thickness t, rectangle width w, and height h, for tuning effective material properties. (d) Homogenized density and in-plane moduli, normalized by water density $\rho_0 = 1000\,\mathrm{kg/m^3}$ and bulk modulus $K_0 = 2.25\,\mathrm{GPa}$, of the designed cloak. Dashed lines represent properties derived from transformation. (e) Geometric parameters corresponding to the five graded unit cells.

Figure 1(a) shows the fabricated annular cloak machined from an aluminum block using an advanced electrical discharge machining technique with high accuracy. The fabricated cloak weighs 4.87 kg and differs about 10% from an ideal one (4.42 kg) [32]. A total of 50 sectors of cells are assembled around the θ direction, and each sector [Fig. 1(b), bounded by red lines] has five graded PM unit cells along the r direction. In designing the cloak, a transformation theory with an optimization algorithm is first used to obtain the principal moduli K_θ and K_r [Figs. 1(d)], and density ρ for cloaking, and then the required material parameters are realized by calibrating the geometry parameters [Fig. 1(e)] of the adopted PM unit cell [Fig. 1(c)] (see Ref. [38]). Different from other unit cells [27], the rectangle mass components are transferred to the middle point of the thin ribs, and therefore further suppress the shear wave by decreasing the rigidity of the rib joints [26], which results in highly anisotropic modulus fluid behavior with a single longitudinal polarized mode (see Fig. S1 in Ref. [38]). Due to the small thickness of this cloak, material properties are obtained with an optimization algorithm to achieve broadband invisibility. A large gradient in the optimized material properties, particularly between the second and fourth layers, on one hand guarantees a satisfying cloaking performance, and on the other hand brings forth significant challenges in the cloak design. The pentamode cells in the corresponding layer should have required effective material parameters and ensure the designed layer thickness as well. Modulus anisotropy K_θ/K_r increases from the outer to the inner sides, reaching 40 for the first two layers, while the outermost layer is nearly impedance matched with water ($Z_{\mathrm{cloak}}/Z_{\mathrm{water}} = 0.94$; Z represents impedance).

Since the cloak is based on a two-dimensional design, a cloak with large axial dimension is more appropriate

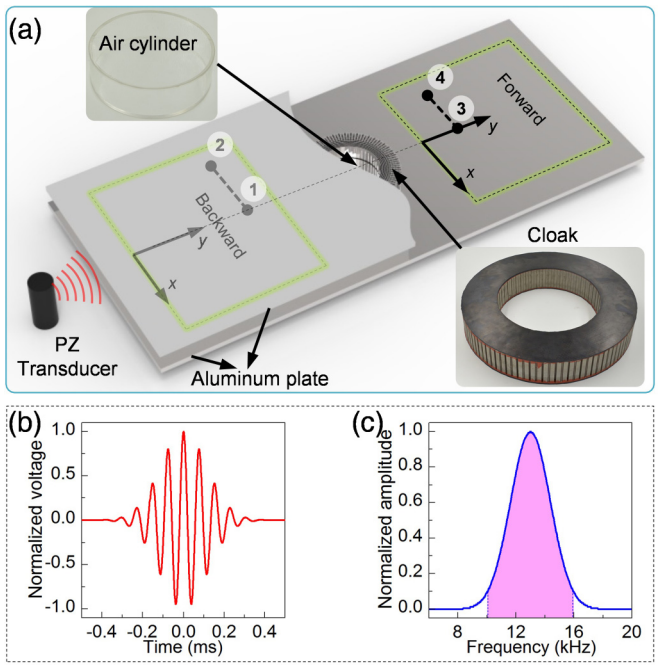

FIG. 2. Experiment setup for underwater acoustic tests. (a) 2D underwater acoustic waveguide composed of two opposing aluminum plates and transducer. Part of the upper plate is removed to show the scatter and cloak position for the experiment. Inset figures show the air cylinder used as scatter and the rubber covered cloak. Forward and backward regions (600 × 560 mm) are 450 mm apart. Locations 1 and 3 lie along the central line of the waveguide and are 475 mm away from the center, while locations 2 and 4 are 200 mm from 1 and 3, respectively. (b), (c) Time and frequency plots of Gaussian burst with central frequency 13 kHz and time duration 0.7 ms used for driving the transducer.

for experiment tests. Limited by machining capability, the fabricated cloak is of a small size, 50 mm in the z direction, and therefore experiment tests should be conducted in a 2D underwater waveguide, which can verify the invisibility effect of the fabricated cloak as if it is infinite in the z direction. However, designing 2D underwater waveguides is not trivial, since the large water density excludes any solid plate of feasible thickness from serving as an acoustic rigid boundary. Therefore, we propose a 2D underwater waveguide based on pressure compensation. The waveguide was composed of two opposing aluminum plates and a cylindrical piezoelectric transducer (PZT) immersed in an anechoic water pool [Fig. 2(a)]. The cloak and scatter were mounted in the middle of the waveguide chamber. To keep the voids in the cloaking shell free of water, the top and bottom cloak surfaces were sealed with 4-mm-thick water matched rubber. A thin walled polymethyl methacrylate hollow cylinder (diameter 200 mm and height 50 mm) was used as the scatter, which can be treated as air scatter with extremely small density.

Since the cloak is expected to work over broadband frequency, transient wave excitation rather than steady wave of a single frequency is preferred. We adopted a Gaussian burst of form $\exp[-0.222(f_c t)^2]\cos(2\pi f_c t)$ to drive the PZT, where f_c denotes the central frequency. Figure 2(b) shows the driven signal for $f_c = 13$ kHz, which lasts 0.7 ms to distinguish between incident and reflective signals. At this central frequency, one wavelength is approximately 11 largest unit cells of the cloak, so the homogenization condition holds. The frequency transformed signal [Fig. 2(c)] spans from 10 to 16 kHz with amplitude larger than 10% of the central frequency amplitude, hence the broadband performance of the cloak can be verified. In the experiment, acoustic pressure fields corresponding to the forward and backward regions [Fig. 2(a)] inside the waveguide for three cases (see Fig. S2 in Ref. [38])—

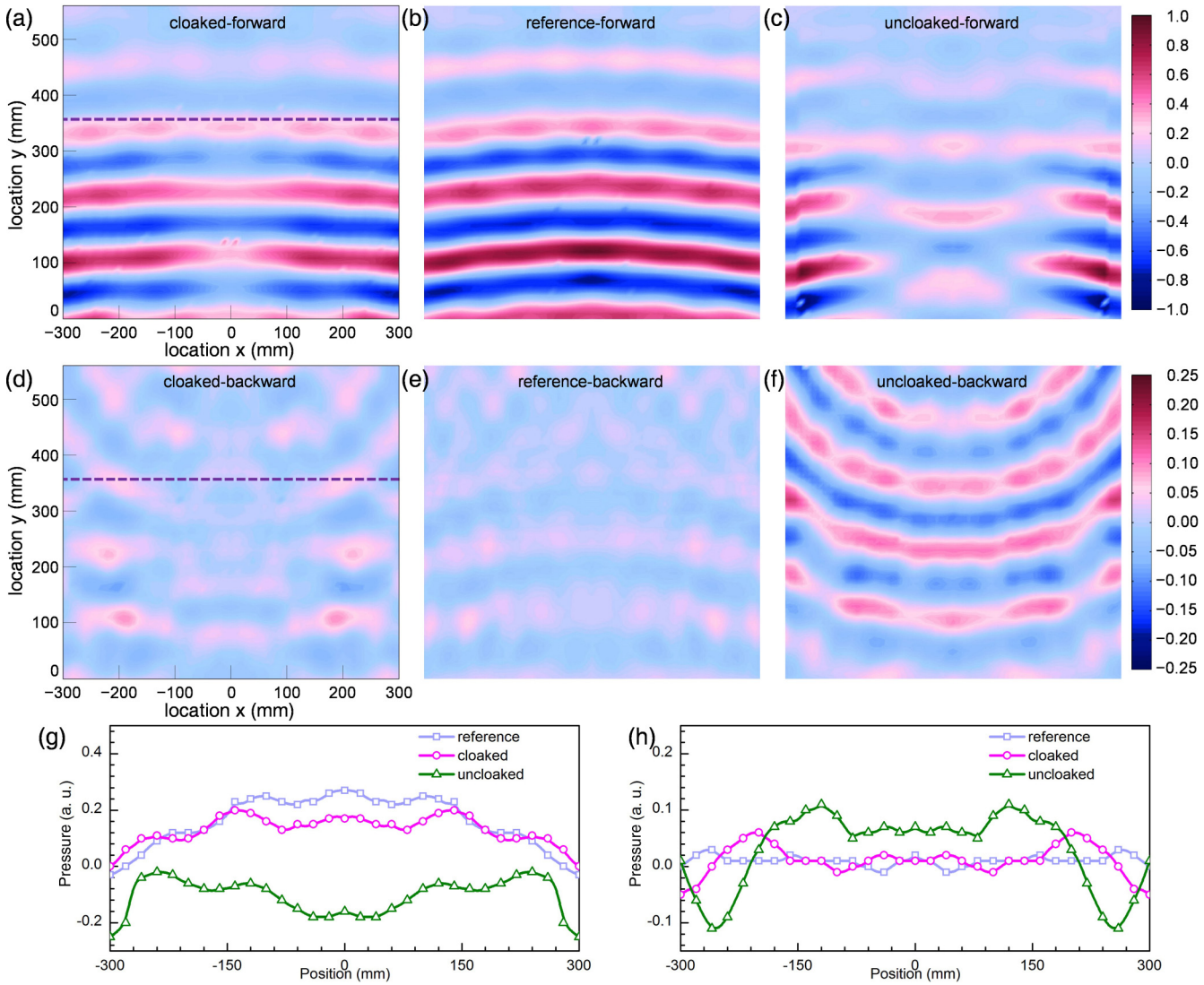

FIG. 3. Measured pressure under incidence of cylindrical Gaussian wave. (a)–(c) Instantaneous pressure fields in the forward region for the cloaked, reference, and uncloaked cases, respectively. (d)–(f) The same as in (a)–(c) but for the backward region. The cylindrical Gaussian wave is incident from the bottom. Pressure in the forward/backward region was normalized by the largest absolute pressure of the reference case in the forward/backward region. (g), (h) Pressure distribution for the three cases along the indicated horizontal line $y = 350$ mm in forward and backward regions, respectively.

reference (empty waveguide), uncloaked scatter, and cloaked scatter—were scanned using a hydrophone moving along orthogonal axes with 10 mm steps. 3D numerical simulations have been conducted to validate the proposed waveguide with pressure compensation (see Figs. S2 and S3 in Ref. [38]).

Measured snapshots of pressure fields in the forward region are shown in Figs. 3(a)–3(c). For the reference case [Fig. 3(b)], pressure fields show nearly undisturbed cylindrical wave form as expected, and this provides a measurement benchmark. For the uncloaked scatter case [Fig. 3(c)], the impinging cylindrical wave is mostly blocked due to significant impedance mismatch with water, and a clear shadow is formed behind the scatter. A small amount of energy flows around the scatter from the lateral side, inducing phase lag owing to the longer propagation trajectory. When the scatter is covered with the cloak [Fig. 3(a)], impinging acoustic energy is directed by graded material properties to the forward region, substantially eliminating the acoustic shadow to the reference case [Fig. 3(b)]. Pressures [Fig. 3(g)] along the indicated horizontal line in the forward region also show a very similar result for the empty waveguide and cloaked scatter cases.

As for pressure in the backward region [Figs. 3(d) and 3(e)], a reflected wave is only clearly observed for the uncloaked case [Fig. 3(f)] after the incident wave has passed through this region. The cloaked case shows much less reflection [Fig. 3(d)] and absolute pressure along the indicated line remains at the same level as the reference case [Fig. 3(h)]. Experimentally measured pressure fields in the forward and backward regions both also agree very well with numerical simulations (see Fig. S4 in Ref. [38]). The enhanced forward transmission and reduced backward reflection can be more clearly seen from the measured transient pressure fields (see Video S1 in Ref. [38]). These results prove the impedance match of the cloak with water, and also indicate excellent cloaking effect for the enclosed scatter. Further experiments on aluminum cylinder scatter also validated the proposed underwater waveguide (see Fig. S5 and Video S5 in Ref. [38]).

Figures 4(a)–4(d) show the pressures measured at locations 1–4 in Fig. 2(a), respectively. At backward location 1 [Fig. 4(a)], the incident Gaussian packets for all three cases are similar, whereas the reflected Gaussian packet immediately following the incident packet is only clearly seen for the uncloaked case. The reflected signal partly overlaps with the incident one due to large water wave velocity, and is significantly reduced when cloaked. This suppressing effect for the reflected signal is more clearly identified at another backward location [Fig. 4(b)]. At forward location 3 [Fig. 4(c)], the uncloaked case shows weaker and phase retarded signals as expected, and the phase retardation is rectified with moderate amplitude recovery while cloaked. Forward location 4 [Fig. 4(d)] shows perfect restoration for both amplitude and phase with the cloak.

Finally, we quantified the broadband efficiency of the designed cloak using target strength reduction (TSR), calculated from the reflective signal strength. The TSR with a covered cloak can be obtained as $10 \times \log_{10}(E_{cl}/E_{un})$, where E_{cl} and E_{un} represent the energy of the reflective signal for the uncloaked and cloaked cases, respectively. Additional experiments using signals with different central frequencies were conducted to cover a wide frequency band (see Videos

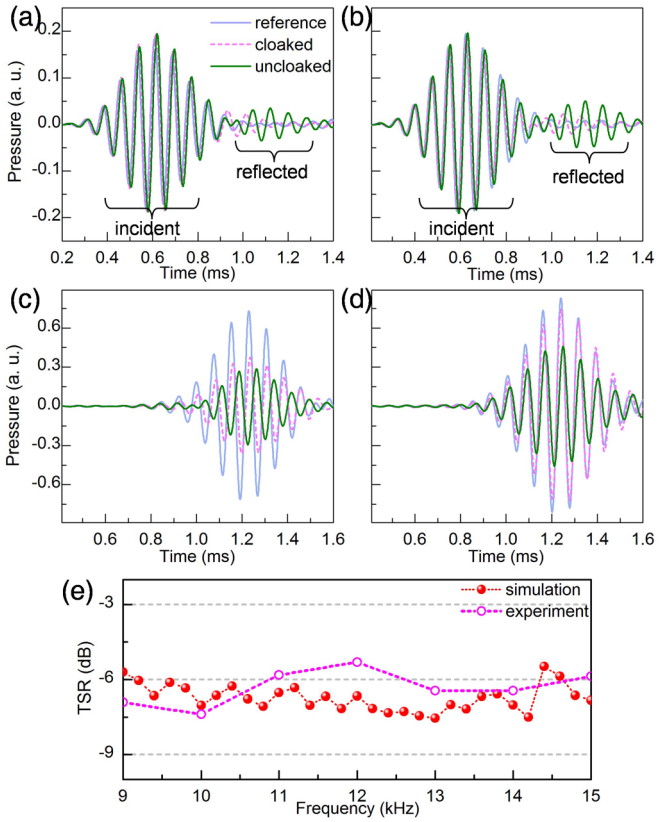

FIG. 4. Cloaking performance. (a), (b) Pressure measured at backward locations 1 and 2 from Fig. 2(a). (c), (d) As (a) and (b) for forward locations 3 and 4 in Fig. 2(a). (e) Simulated and measured cloaked TSR for 9–15 kHz.

S2–S4 in Ref. [38]). Reflective signals for both cases were taken from location 2 rather than 1 to calculate the TSR with clearly distinguished reflected and incident signals. In the studied frequency range, the simulated TSR [Fig. 4(e)] is nearly constant with small peaks caused by shear resonance scattering [26]. The overall trend of the measured TSR is consistent with the simulation, where differences may arise from system errors including fabrication, measurement, and imperfect waveguide. The experiment validates the superior stealth capability of the designed cloak, achieving 6.3 dB average reduction within a remarkably broad frequency range of 9–15 kHz. It should be noted, although measurements here only indicate the excellent performance of the designed cloak over the given range owing to transducer frequency limitations, the designed cloak can in principle work from zero frequency, since only quasistatic material properties are employed [26], in contrast to cloaks based on resonance mechanisms [3,6].

In conclusion, we have experimentally demonstrated a broadband solid cloak for underwater acoustics within a designed 2D underwater waveguide. The cloak is composed of a highly anisotropic pentamode solid material, which acts as an anisotropic modulus metafluid and acquires much stronger anisotropy than any anisotropic density metafluid in water. The high anisotropy in the modulus enables a favorable thinner cloak layer, and also provides excellent cloaking for the enclosed object attributed to the near impedance match and strongly bending capability for the acoustic wave. The

solidity, broadband, and easy tuning feature of pentamode materials offer new possibilities to control underwater acoustic waves with unprecedented flexibility. Many applications for underwater acoustics may arise from this concept, such as acoustic radiation shaping, elastic/acoustic energy transforming devices, etc.

The authors would like to thank H. Jia for discussions on waveguide design, and X. Ruan for preparing part of the hardware devices. Funding support from the Natural Science Foundation (Grants No. 11472044, No. 11221202, No. 11632003 and No. 11521062) and from 111 Project (B16003) is acknowledged.

[1] J. B. Pendry, D. Schurig, and D. R. Smith, Science **312**, 1780 (2006).
[2] U. Leonhardt, Science **312**, 1777 (2006).
[3] D. Schurig, J. J. Mock, B. J. Justice, S. A. Cummer, J. B. Pendry, A. F. Starr, and D. R. Smith, Science **314**, 977 (2006).
[4] W Cai, U. K. Chettiar, A. V. Kildishev, and V. M. Shalaev, Nat. Photonics **1**, 224 (2007).
[5] B. Edwards, A Alù, M. G. Silveirinha, and N. Engheta, Phys. Rev. Lett. **103**, 153901 (2009).
[6] R. Liu, C. Ji, J. J. Mock, J.Y. Chin, T. J. Cui, and D. R. Smith, Science **323**, 366 (2009).
[7] J. Valentine, J. Li, T. Zentgraf, G. Bartal, and X. Zhang, Nat. Mater. **8**, 568 (2009).
[8] B. Zhang, Y. Luo, X. Liu, and G. Barbastathis, Phys. Rev. Lett. **106**, 033901 (2011).
[9] N. Landy and D. R. Smith, Nat. Mater. **12**, 25 (2013).
[10] N. Stenger, M. Wilhelm, and M. Wegener, Phys. Rev. Lett. **108**, 014301 (2012).
[11] D. Misseroni, D. J. Colquitt, A. B. Movchan, N. V. Movchan, and I. S. Jones, Sci. Rep. **6**, 23929 (2016).
[12] H. Xu, X. Shi, F. Gao, H. Sun, and B. Zhang, Phys. Rev. Lett. **112**, 054301 (2014).
[13] T. Han, X. Bai, D. Gao, J. T. L. Thong, B. Li, and C. W. Qiu, Phys. Rev. Lett. **112**, 054302 (2014).
[14] D. R. Smith, W. J. Padilla, D. C. Vier, S. C. Nemat-Nasser, and S. Schultz, Phys. Rev. Lett. **84**, 4184 (2000).
[15] M. Farhat, S. Enoch, S. Guenneau, and A. B. Movchan, Phys. Rev. Lett. **101**, 134501 (2008).
[16] Z. Liu, X. Zhang, Y. Y. Zhu, Z. Yang, C. T. Chan, and P. Sheng, Science **289**, 1734 (2000).
[17] S. A. Cummer and D. Schurig, New J. Phys. **9**, 45 (2007).
[18] H. Chen and C. Chan, Appl. Phys. Lett. **91**, 183518 (2007).
[19] B. I. Popa, L. Zigoneanu, and S. A. Cummer, Phys. Rev. Lett. **106**, 253901 (2011).
[20] L. Zigoneanu, B. I. Popa, and S. A. Cummer, Nat. Mater. **13**, 352 (2014).
[21] J. B. Pendry and J. Li, New J. Phys. **10**, 115032 (2008).
[22] D. Torrent and J. Sanchez-Dehesa, Phys. Rev. Lett. **105**, 174301 (2010).
[23] Y. Urzhumov, F. Ghezzo, J. Hunt, and D. R. Smith, New J. Phys. **12**, 73014 (2010).
[24] B. I. Popa, W. Wang, A. Konneker, S. A. Cummer, and C. A. Rohde, J. Acoust. Soc. Am. **139**, 3325 (2016).
[25] S. Zhang, C. Xia, and N. Fang, Phys. Rev. Lett. **106**, 024301 (2011).
[26] Y. Chen, X. Liu and G. Hu, Sci. Rep. **5**, 15745 (2015).
[27] C. N. Layman, C. J. Naify, T. P. Martin, D. C. Calvo, and G. J. Orris, Phys. Rev. Lett. **111**, 024302 (2013).
[28] A. C. Hladky-Hennion, J. O. Vasseur, G. Haw, C. Croënne, L. Haumesser, and A. N. Norris, Appl. Phys. Lett. **102**, 144103 (2013).
[29] A. Martin, M. Kadic, R. Schittny, T. Bückmann, and M. Wegener, Phys. Rev. B **86**, 155116 (2012).
[30] M. Kadic, T. Bückmann, N. Stenger, M. Thiel, and M. Wegener, Appl. Phys. Lett. **100**, 191901 (2012).
[31] G. W. Milton and A. V. Cherkaev, J. Eng. Mater. Technol. **117**, 483 (1995).
[32] A. N. Norris, Proc. R. Soc. London, Ser. A **464**, 2411 (2008).
[33] C. L. Scandrett, J. E. Boisvert, and T. R. Howarth, J. Acoust. Soc. Am. **127**, 2856 (2010).
[34] J. Cipolla, N. Gokhale, A. N. Norris, and A. Nagy, J. Acoust. Soc. Am. **130**, 2332 (2011).
[35] Y. Tian, Q. Wei, Y. Cheng, Z. Xu, and X. Liu, Appl. Phys. Lett. **107**, 221906 (2015).
[36] X. Cai, L. Wang, Z. Zhao, A. Zhao, X. Zhang, T. Wu, and H. Chen, Appl. Phys. Lett. **109**, 131904 (2016).
[37] Y. Chen, X. Liu, and G. Hu, J. Acoust. Soc. Am. **140**, EL405 (2016).
[38] See Supplemental Material at http://link.aps.org/supplemental/10.1103/PhysRevB.95.180104 for details on the cloak design and experiment setup, additional analysis on the proposed underwater waveguide, calculations, and videos, which includes Refs. [39–42].
[39] N. H. Gokhale, J. L. Cipolla, and A. N. Norris, J. Acoust. Soc. Am. **132**, 2932 (2012).
[40] A. S. Titovich and A. N. Norris, J. Acoust. Soc. Am. **136**, 1601 (2014).
[41] W. Chen, Z. Bian, and H. Ding, Int. J. Mech. Sci. **46**, 159 (2004).
[42] D. N. MacLennan and E. J. Simmonds, *Fisheries Acoustics* (Springer, New York, 2013).